Geomechanics and Engineering, *Vol. 33, No. 1 (2023) 53-63*
https://doi.org/10.12989/gae.2023.33.1.053

Stability analysis of infinite rock slopes with varying disturbances based on the Hoek–Brown failure criterion

Dowon Park*

Department of Civil Engineering, University of Seoul,
163 Seoulsiripdae-ro, Dongdaemun-gu, Seoul 02504, Republic of Korea

(*Received November 25, 2022, Revised February 22, 2023, Accepted March 7, 2023*)

Abstract. Rock disturbance caused by blasting and stress relaxation is commonly observed during excavation. As the distance from the source of disturbance increases, the degree of disturbance decreases, and rock at a large depth does not experience disturbance. However, in stability analyses, a single value of disturbance is often applied to the entire rock mass, which leads to underestimated results. In this study, this modeling mistake is addressed by considering realistically varying rock disturbance. The safety of infinite slopes in a disturbed rock mass with a strength governed by the Hoek–Brown failure criterion is investigated based on the kinematic approach of limit analysis. The maximum disturbance is assigned to the outermost slope face because it is directly exposed to blasting damage and dilation, and the disturbance progressively decays with distance in the rock mass. The safety analysis results indicate that the assumption of uniform disturbance in the entire rock mass leads to underestimation of the rock strength and safety on infinite rock slopes. A critical slip surface appears to be within the disturbed rock layer as well as the interface between the disturbed upper rock and undisturbed lower rock.

Keywords: Hoek–Brown failure criterion; infinite slope; limit analysis; rock disturbance; rock slope stability

1. Introduction

Most rock structures, such as slopes, foundations, tunnels, and underground cavities, are excavated using blasting and drilling. These procedures inevitably induce rock disturbances caused by blasting damage and stress relaxation around the excavation, thereby weakening the strength of the rock mass and the safety of the rock structure (Cheng *et al.* 2021, Chinaei *et al.* 2021, Dimitraki *et al.* 2021, Zaid *et al.* 2020). Hoek and Karzulovic (2000) observed that a potentially disturbed zone can expand up to 100 m behind the slope face for very large slopes that require several tons of explosives for excavation. Dilation of rocks caused by stress redistribution is also a major concern. According to field observations of unconfined rock surfaces (Chern *et al.* 1998, Hoek and Karzulovic 2000, Sakurai 1984), only 1%–2% of the strain can cause a complete loss of the cohesive strength of the rock, which could lead to a residual state. Attempts for the quantitative characterization of rock disturbance have been focused on the magnitude of rock disturbance (Hoek and Brown 2019, Hoek *et al.* 2002, Sonmez and Ulusay 1999); extent of the disturbed zone (Hoek and Karzulovic 2000, Kwon *et al.* 2009, Yang *et al.* 2020), and disturbance decay patterns with increasing distance from the source of disturbance (Lupogo 2017, Rose *et al.* 2018, Yang *et al.* 2020).

Although these factors are important, this study focuses on the demonstration of infinite rock slope analysis accounting for spatially varying rock disturbances.

The face in the vicinity of an excavation is maximally disturbed, and the degree of disturbance progressively decreases with increasing distance from the source. However, many studies, including previous and recent ones, assumed a uniform disturbance in the entire rock mass, which resulted in a significant underestimation of the slope stability (Dong-ping *et al.* 2016, Sun *et al.* 2016). Hoek (2012) suggested that the same degree of blast damage should not be applied to the entire rock mass but only to the actual damage zone. Li *et al.* (2011) numerically showed that the safety of a uniformly (fully) disturbed rock slope can be underestimated by 50% compared to that of a rock slope with varying disturbances. To consider the progressively diminishing disturbance away from the slope face, the disturbed zone behind the slope face was divided into several layers, and decreasing disturbance values were sequentially assigned to these layers. Later, the parallel layer model (PLM) was proposed based on this approach (Zheng *et al.* 2018). This technique has been adopted for studies based on finite element analyses owing to its straightforward implementation of varying rock disturbances in the mesh (Qian *et al.* 2017, Yang *et al.* 2020).

In this study, the influence of the decaying rock disturbance with distance from the disturbance source on slope safety was analyzed. Instead of a stepwise decrease in disturbance based on the PLM, a continuous function was employed through a semi-analytical technique. An infinite rock slope in which a rock mass slides on the failure surface parallel to the slope face was explored.

In geotechnical engineering, the safety assessment of infinite slopes is an important task (Rankine 1857). Most

*Corresponding author, Assistant Professor,
E-mail: dowon@uos.ac.kr

ISSN: 2005-307X (Print), 2092-6219 (Online)

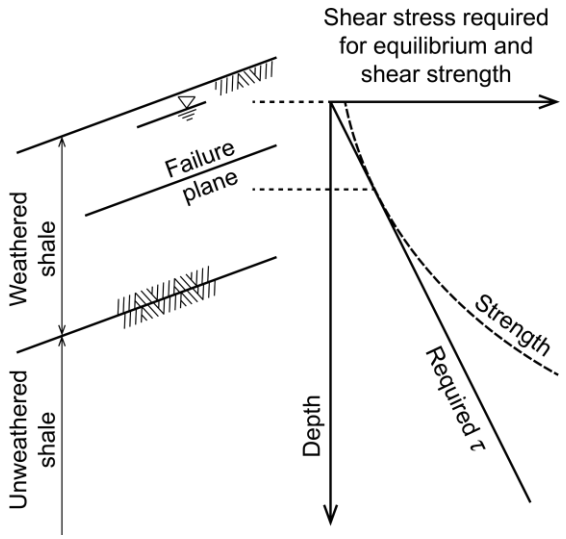

Fig. 1 Development of a slip surface within weathered rock (after Lambe and Whitman (1969))

textbooks cover this topic (Das 2021, Duncan *et al.* 2014, Lambe and Whitman 1969) owing to the simplicity of the analysis and insights into slope stability. However, the literature regarding rock masses with strength governed by nonlinear failure criteria is rare, and the spatial distribution of rock properties, such as disturbance, has not been considered (Michalowski 2018, Serrano *et al.* 2005). A common example of infinite rock slope failure was demonstrated by Lambe and Whitman (1969), as illustrated in Fig. 1. Intact and unweathered rocks underlie the upper weathered rock masses. The shear strength of the upper rock layer is reduced by the weathering process (or disturbance), resulting in unequal strength parameters as the depth increases. In such a case, a critical slip surface associated with the most adverse conditions must be searched, probably within the weathered rock mass. Infinite slope failure at the interface between a weak upper rock and strong lower bedrock is also a common occurrence. The novelty of this study lies in the stability analysis of infinite slopes in disturbed rocks and the search for a potential slip surface located within the upper disturbed layer.

The kinematic approach of limit analysis was used as a stability assessment method for infinite rock slopes with strength governed by the Hoek–Brown failure criterion. The criterion accounts for rock disturbance using a descriptor depending on the blasting control and excavation methods. A brief explanation of the Hoek–Brown criterion and rock disturbance is provided in Sections 2 and 3, respectively. In Section 4, a kinematically admissible failure mechanism for infinite slopes is postulated, and a safety analysis is performed. The computational results and discussion are presented in Section 5, followed by the conclusions in Section 6.

2. Hoek–Brown failure criterion

The peak strength of rock exhibits a nonlinear dependency on pressure, and nonlinear failure criteria are

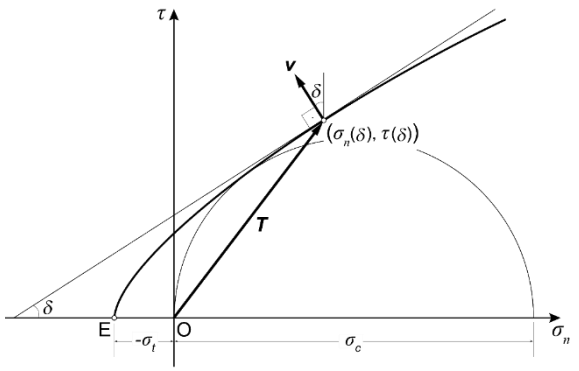

Fig. 2 Hoek–Brown failure criterion

preferred in stability analysis in rock engineering. Among them, the Hoek–Brown failure criterion (Hoek and Brown 1980, Hoek *et al.* 2002) is most widely accepted based on extensive experience gained from diverse engineering projects around the world over 40 years. The Hoek–Brown failure criterion for the principal stress plane (expressed as total stress terms) is expressed as an empirical relationship between σ_1 and σ_3 as follows

$$\sigma_1 = \sigma_3 + \sigma_{ci}\left(m_b \frac{\sigma_3}{\sigma_{ci}} + s\right)^a \tag{1}$$

where σ_{ci} is the uniaxial compressive strength of intact rock, and m_b, a, and s are constants (curve fitting parameters) calculated as follows

$$m_b(y) = m_i e^{\left(\frac{GSI-100}{28-14D(y)}\right)} \tag{2}$$

$$a = \frac{1}{2} + \frac{1}{6}\left(e^{-\frac{GSI}{15}} - e^{-\frac{20}{3}}\right) \tag{3}$$

$$s(y) = e^{\left(\frac{GSI-100}{9-3D(y)}\right)} \tag{4}$$

where m_i, GSI, and D are the rock-type-dependent parameter, geological strength index, and disturbance factor, respectively. In this study, the disturbance factor D is represented by a spatially varied function with coordinate y defined in Section 3; therefore, constants m_b and s are also functions of y. The most recent discussion on the Hoek–Brown criterion, including its applications, case histories, selection guidelines of the parameters, and limitations, is found in the paper by Hoek and Brown (2019).

Fig. 2 illustrates the Hoek–Brown criterion defined in $\sigma_1 - \sigma_3$ space. σ_c and σ_t are the uniaxial compressive strength and isotropic tensile strength, respectively. It is recommended that these strengths be directly measured by proper laboratory testing; however, they are often determined (predicted) from the failure envelope without justification.

Based on the geometric relations in Fig. 2, σ_c and σ_t are calculated by substituting $\sigma_1 = \sigma_c$ and $\sigma_3 = 0$, and $\sigma_1 = \sigma_3 = -\sigma_t$ into Eq. (1), respectively

$$\sigma_c = \sigma_{ci} s^a \tag{5}$$

$$\sigma_t = \sigma_{ci} \frac{s}{m_b} \tag{6}$$

where m_b, a, and s are expressed in Eqs. (2)-(4), respectively. For intact rock with a *GSI* of 100, the uniaxial compressive strength of the rock mass in Eq. (5) is equal to σ_{ci}, and the isotropic tensile strength in Eq. (6) is reduced to σ_{ci}/m_i.

The utilization of the kinematic limit analysis requires the Mohr envelope defined in $\tau - \sigma_n$ space. Although a closed-form expression is unavailable thus far, Eq. (1) can be alternatively expressed in parametric form with respect to the tangent angle δ (Balmer 1952, Kumar 1998)

$$\sigma_n = \sigma_{ci} \left\{ \left(\frac{1}{m_b} + \frac{\sin\delta}{m_b a} \right) \left[\frac{m_b a (1-\sin\delta)}{2\sin\delta} \right]^{\frac{1}{1-a}} - \frac{s}{m_b} \right\} \tag{7}$$

$$\tau = \sigma_{ci} \left\{ \frac{\cos\delta}{2} \left[\frac{m_b a (1-\sin\delta)}{2\sin\delta} \right]^{\frac{a}{1-a}} \right\} \tag{8}$$

This parametric Hoek–Brown equation was used in this study rather than the original failure criterion in Eq. (1), which has no closed-form expression for the shear strength envelope; both convey the same information.

3. Rock disturbance

The first version of the Hoek–Brown criterion (Hoek and Brown 1980) did not consider rock disturbance; an updated Hoek–Brown criterion in 1988 (Hoek and Brown 1988) introduced the concept of disturbed rocks to consider stress relaxation and blasting using a different set of equations for calculating the Hoek–Brown constants. In 1994, the equation for disturbed rock was removed; instead, rock disturbance was indirectly considered from a reduced geological strength index (*GSI*), which is a newly introduced parameter of the version (Hoek 1994). However, one of the practical problems in the version was the estimation of the *GSI* in the field where the rock has experienced blast damage, as indicated by Hoek and Brown (1997). By 2002 (Hoek *et al.* 2002), the influence of disturbances became increasingly important in rock engineering projects owing to widespread heavy blasting, and a new parameter D was explicitly introduced to the criterion and embedded in parameters m_b and s, as shown in Eqs. (2) and (4). respectively. More details on the disturbance factor and a series of modifications to the Hoek–Brown criterion are provided in the reports by Hoek (2012) and Hoek and Marinos (2007), respectively.

Although it is apparent that the disturbance factor ranges from 0 (undisturbed rock) to 1 (fully disturbed rock), its exact value in the field is a matter of judgment. A practical guideline for selection has been provided since its inception (Hoek *et al.* 2002). In the most recent version, Hoek and Brown (2019) suggested that D = 0 can be used for excellent quality-controlled blasting or excavation by machines (mechanical excavation), and D = 0.5, which is appropriate for controlled presplit or small-scale blasting; D = 0.7 for mechanical excavation effects of stress reduction damage (ripping and dozing); and D = 1 for heavy production blasting (or poor blasting) and stress relief from overburden removal. While typical rock properties follow random field models (Hsu and Nelson 2006, Rafiei Renani *et al.* 2019, Song *et al.* 2011), it is expected that the rock disturbance decays with the distance away from the disturbance source. Consequently, the influential depth owing to the disturbance and its spatial variation are also of critical importance. Based on experience in open-pit mine slopes (Hoek and Karzulovic 2000), the thickness of the blast damage zone can be related to the slope height (H); the influential thickness by blasting is within the range of 0.3 to 2.5H, depending on the blast control and free surface. In another study (Yang *et al.* 2020), field measurements of damage zones in rock slopes after blasting presented 1.5 – 4 m of disturbed thickness. Regarding a tunnel with 10 m span, rock disturbance can affect the surrounding rock to a depth of 2 – 3 m (Kwon *et al.* 2009, Yang *et al.* 2020). Most studies have assumed a simple linear decrease in the disturbance factor away from the maximally disturbed surface within the disturbed zone (Li *et al.* 2011, Zheng *et al.* 2018). Recently, acoustic tests performed by Yang *et al.* (2020) on rock slopes presented a linear reduction in the disturbance factor; however, a different decaying pattern was also supported by other studies, for example, exponentially decreasing rock disturbance in rock mass (Lupogo 2017, Rose *et al.* 2018). The spatial variation of the disturbance factor is still not clear as experimental evidence is insufficient; thus, a general function capable of various distributions of the disturbance factor was utilized in this study.

The Hoek–Brown failure envelopes with different disturbance factors D = 0, 0.5, and 1 are illustrated in Fig. 3(a). As expected, the disturbance factor had a significant impact on the rock strength. Both the shear and tensile strengths of the undisturbed rock mass were consistently higher than those of the disturbed rock in all stress ranges. The substantial strength drop caused by the rock disturbance indicates that the overall behavior of the rock mass is strongly dependent on the disturbance quantified by the disturbance factor D.

The Hoek–Brown constants m_b and s are functions of *GSI* as well as D. Because of the form in Eqs. (2) and (4), the influence of factor D on these parameters can be large or small depending on the *GSI*. This is demonstrated in Fig. 3(b), where the Hoek–Brown strength criteria for undisturbed and "fully" disturbed rocks are presented for different *GSI* values of 10, 50, and 90. The relative strength difference between rocks with D = 0 and D = 1 decreases with an increase in the *GSI*; the forms of coefficients m_b and s in Eqs. (2) and (4) were chosen such that factor D had no influence on the rock strength when *GSI* = 100. The disturbance factor is particularly important in weak rock masses characterized by low GSI values. Table 1 lists the uniaxial compressive strengths of the rocks with different disturbance factors and *GSI* values. In the case of a "fully"

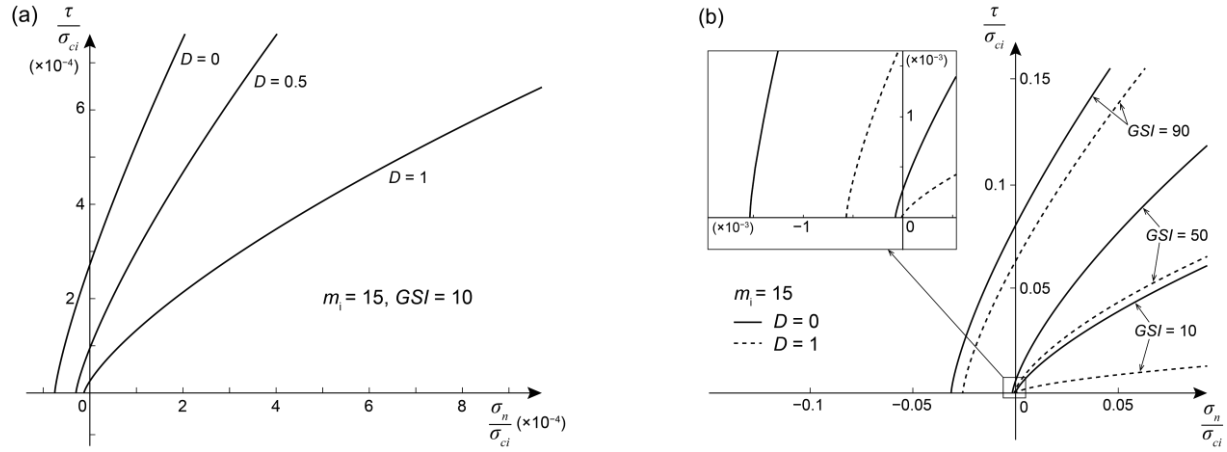

Fig. 3 Hoek–Brown strength envelopes with different disturbance factors D: (a) strength envelopes for D = 0, 0.5, and 1 on $\tau - \sigma_n$ plane and (b) comparison of strength envelopes for undisturbed and fully disturbed rock with GSI = 10, 50, and 90

Table 1 Normalized uniaxial compressive strength σ_c/σ_{ci} of disturbed rock mass (m_i = 15)

D	GSI			
	10	40	70	100
0	0.00287	0.03307	0.18802	1*
0.5	0.00089	0.01672	0.13460	1*
1	0.00015	0.00601	0.08153	1*

*$\sigma_c = \sigma_{ci}$ for intact rock (GSI = 100)

disturbed rock mass (D = 1) with GSI = 10, the strength was reduced by 94.6% relative to that of the undisturbed rock mass (D = 0).

4. Failure mechanism and stability analysis

4.1 Failure mechanism

Fig. 4 shows a schematic of an infinite slope in a disturbed rock mass. As the name indicates, the slope has an infinite extent, with a slip surface parallel to the slope face. The depth of the sliding rock mass is very small compared with the lateral length of the slope. The scaling parameter of slope T_0 is the thickness of the disturbed zone (or distance to the undisturbed rock from the slope face). The failure surface with thickness T can be located inside the disturbed rock ($0 < T \leq T_0$) and is not determined a priori. This is the outcome of the analysis.

Rock strength is governed by the Hoek–Brown failure criterion (Eq. (1)). The rock is maximally disturbed at the slope face owing to blasting and stress relief, and the degree of disturbance decreases with depth y away from the maximum disturbance. In this study, the following general function of the disturbance decay rate was adopted to examine the influence of rock disturbance

$$D(y) = D_{max}\left[1 - \left(\frac{y}{T_0}\right)^k\right] \tag{9}$$

where D_{max} is the maximum disturbance, y is the distance from the slope face, k is the power of different disturbance-decaying functions, and T_0 is the thickness of the disturbed rock. The linear decaying function of rock disturbance, frequently assumed in the literature (Li *et al.* 2011, Zheng *et al.* 2018), is a special case of Eq. (9) when k = 1.

For uniform slopes with homogeneous rock properties, the thickness of the moving mass T can be considered equal to T_0. For rock masses with varying disturbances with depth, it is not necessarily identical; the slip surface can be formed at any depth in the rock associated with the most adverse condition. The disturbance factor D (T) is used in the analysis because the slip surface is at a distance T from the slope face.

The postulated failure mechanism is constructed by a continuum-based analysis, where Eq. (1) is applicable: the rock mass is assumed to be continuous and isotropic without weak discontinuities. As a result, the slope failure is not structurally controlled but governed by the most unfavorable (critical) failure mechanism giving the best bounds to the safety measures. No hydraulic influence was accounted for, but the procedure proposed in this study can be applied to infinite rock slopes with seepage flow.

4.2 Stability analysis

The kinematic approach of limit analysis, commonly referred to as the upper-bound theorem, is used as a stability assessment method for infinite slopes. The fundamental assumptions are perfect plasticity, convex yield conditions, and the normality flow rule. The method provides an upper bound to the true failure load, as the failure is either imminent or occurs in the kinematically admissible failure mechanism. The application of limit analysis to rock structures has been reported in recent studies (Michalowski and Park 2020, Park and Michalowski 2019, 2020, 2021, 2022).

By taking the work balance between the rates of dissipated work D_{dis} and external work done by self-weight W_γ, as shown below, one can arrive at a rigorous bound to the true solution.

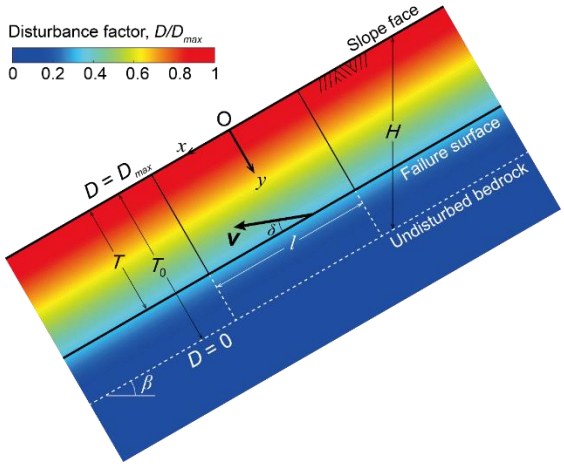

Fig. 4 Schematic of the failure mechanism for an infinite rock slope

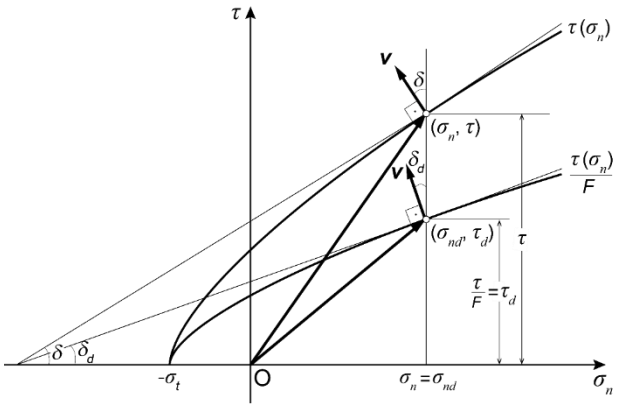

Fig. 5 Hoek–Brown strength envelope and the shear strength reduced by factor of safety F

$$D_{dis} = W_{\gamma} \tag{10}$$

4.2.1 Stability factor

The safety of slopes can be routinely characterized by the stability number, which presents the results in a dimensionless manner (Taylor 1937). Its reciprocal (although it contains the same information) is referred to as the stability factor, also known as the dimensionless critical height. The stability factor is defined as the geomaterial's properties and problem dimension under consideration, and is defined by

$$\left(\frac{\gamma T}{\sigma_{ci}}\right)_{crit} \tag{11}$$

where γ is the unit weight of the rock, σ_{ci} is the uniaxial compressive strength of the intact rock, and T is the layer thickness. In Eq. (11) the classically employed slope height H is not adopted, and it is replaced by thickness T because in infinite slopes, the original expression associated with slope height yields a counter-intuitive outcome (Michalowski 2018).

The stability factors defined in Eq. (11) are associated with the incipient failure (limit state); thus, it can be calculated from the kinematic approach of limit analysis by calculating the minimum value of unsafe loads. The internal dissipated work rate D_{dis} along the unit length l on any slip surface can be determined by

$$D_{dis} = v\left(\tau\cos\delta - \sigma_n \sin\delta\right) l \tag{12}$$

where σ_n and τ are functions of δ, as defined in Eqs. (7) and (8), respectively, where v is the magnitude of the velocity discontinuity vector $\boldsymbol{v}$ on the slip surface. The external work rate of the rock unit weight is derived as

$$W_{\gamma} = \gamma T v \sin(\beta - \delta) l \tag{13}$$

By substituting Eqs. (12) and (13) into the work-balance equation in Eq. (10), one can determine the dimensionless group $\gamma T/\sigma_{ci}$

$$\frac{\gamma T}{\sigma_{ci}} = \frac{\dfrac{\tau}{\sigma_{ci}}\cos\delta - \dfrac{\sigma_n}{\sigma_{ci}}\sin\delta}{\sin(\beta - \delta)} \tag{14}$$

The kinematic approach of the limit analysis yields an upper bound to the true failure load, and the minimum value of Eq. (14) is the stability factor. Finding the critical case associated with the verge of failure involves two variables of optimization, δ and T. The thickness T determines the degree of disturbance on the failure surface, $D(y = T)$ in Eq. (9), and it is embedded in both σ_n and τ terms.

4.2.2 Factor of safety

In addition to the stability factor corresponding to the verge of failure, the factor of safety was also estimated to analyze a given (existing) slope. The factor of safety F is classically defined by the shear strength

$$F = \frac{\tau}{\tau_d} \tag{15}$$

where τ is the rock shear strength and τ_d is the demand on the shear strength required for limit equilibrium.

Fig. 5 illustrates the reduced H-B criterion by F (lower curve), as well as its original envelope (upper curve). Based on the geometric relation, angle δ can be expressed by the corresponding δ_d on the reduced envelope, or vice versa.

$$\delta = \tan^{-1}(F\tan\delta_d) \tag{16}$$

This indicates that for a given angle δ_d, one can calculate the reduced shear strength τ_d from τ (using the calculated angle δ from Eq. (16)) divided by F (Eq. (15)). The computation of the factor of safety involves analysis with a failure mechanism obtained from the envelope reduced by F (lower curve in Fig. 5).

Incorporating the reduced envelope into the analysis, the internal work rate in Eq. (12) can be rewritten as

$$D_{dis} = v\left(\frac{\tau}{F}\cos\delta_d - \sigma_n \sin\delta_d\right) l \tag{17}$$

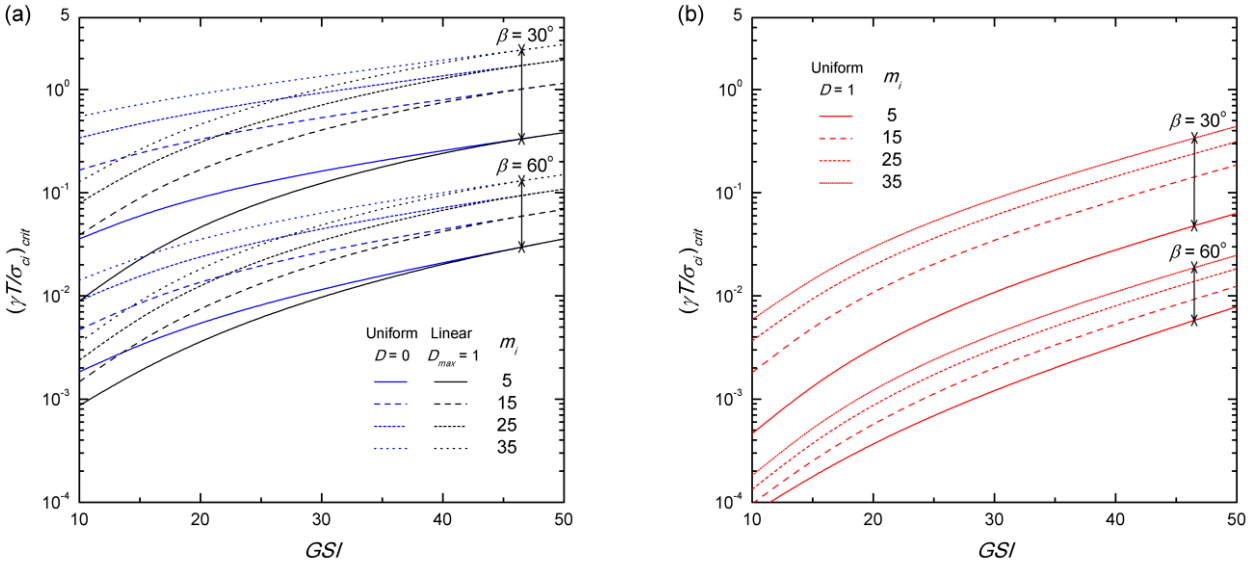

Fig. 6 Stability factor for infinite rock slopes: (a) undisturbed rock (blue) and rock with linearly decaying disturbance factor away from the source of disturbance (black) and (b) fully disturbed rock (red)

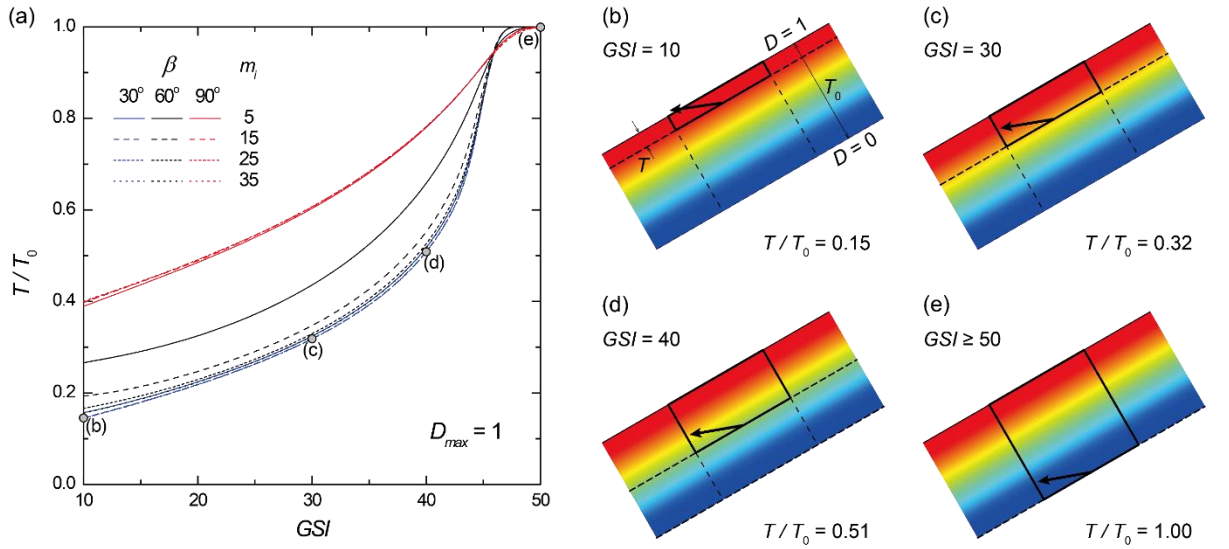

Fig. 7 Influence of *GSI*: (a) normalized thickness of failed rock mass, and failure mechanisms ($\beta = 30°$, $m_i = 15$) with (b) $GSI = 10$, (c) $GSI = 30$, (d) $GSI = 40$ and (e) $GSI = 50$

where σ_n and τ are consistent with those in Eq. (12), where δ is calculated by angle δ_d using Eq. (16). By equating Eq. (17) to the external work rate, Eq. (13), estimated from the reduced failure mechanism (with angle δ_d), the following equation is obtained

$$\frac{\sigma_{ci}}{\gamma T}\left[\frac{1}{F}\frac{\tau}{\sigma_{ci}}\cos\delta_d - \frac{\sigma_n}{\sigma_{ci}}\sin\delta_d\right] = \sin(\beta - \delta_d) \qquad (18)$$

This is an implicit equation with respect to F. When a given rock slope is characterized by a dimensionless number $\sigma_{ci}/\gamma T$, the factor of safety for the slope is computed by solving the implicit equation. The minimum factor of safety among kinematically admissible failure mechanisms must be determined by varying δ_d and T.

5. Results and discussion

Fig. 6 shows the stability factors calculated using Eq. (14), along with the optimization procedure. For clarity, the computational results are plotted in two figures using the same axis scales: undisturbed rock (blue) and rock with linearly decreasing disturbance factor with depth from $D = 1$ at the face and $D = 0$ at T_0 (black) in Fig. 6(a), and fully disturbed rock with $D = 1$ (red) in Fig. 6(b). For weak rocks characterized by a low *GSI* value, the stability factors decrease with an introduced disturbance near the slope face. The influence of the disturbance factor became more substantial with decreasing *GSI*, which is consistent with Fig. 3. It is interesting to note that in Fig. 6(a), the differences in stability factors between undisturbed and disturbed rock with linearly decaying disturbance become negligible when $GSI \geq 50$.

Table 2 Stability factor $(\gamma T/\sigma_{ci})_{crit}$ ($\times 10^{-3}$) for infinite rock slopes with $\beta = 30°$

GSI	Case*	m_i			
		5	15	25	35
10	A	35.77	166.07	341.28	548.68
	B	8.96	38.91	79.61	127.86
	C	0.46	1.81	3.67	5.88
20	A	90.79	332.54	610.79	911.89
	B	47.57	171.68	315.01	470.17
	C	3.19	11.11	20.33	30.32
30	A	162.91	535.27	934.97	1,350.51
	B	125.31	409.33	714.66	1,032.15
	C	10.96	34.91	60.82	87.79
40	A	256.38	797.28	1,359.15	1,932.21
	B	243.32	755.26	1,287.30	1,830.00
	C	28.04	84.95	144.49	205.30
50	A	382.99	1,154.16	1,943.23	2,740.57
	B	382.99	1,154.16	1,943.23	2,740.57
	C	63.41	186.31	312.99	441.16

*Case A: uniform $D = 0$ (undisturbed); Case B: $D_{max} = 1$ and $k = 1$ (linear); Case C: uniform $D = 1$ (fully disturbed)

The much smaller stability factors in Fig. 6(b) compared with those in Fig. 6(a) indicate that assuming a fully disturbed rock without considering naturally diminishing disturbance factors significantly underestimates the safety of infinite rock slopes. The maximum difference in the stability factor between the linearly decreasing disturbance factor and uniform disturbance factor in the entire rock mass can be as high as 20 times. For a quantitative comparison, numerical numbers for the three different disturbance cases are given in Table 2; the results with the blue, black, and red colors in Fig. 6 correspond to Cases A, B, and C in Table 2, respectively. As expected, the stability factors for Case B, rock with a linearly decreasing disturbance factor with depth, were bounded by two extreme cases: Case A (undisturbed rock) and Case C (fully disturbed rock).

Regarding rock masses with varying strength parameters with depth, a slip surface can be located within the upper rock mass in addition to the interface, as illustrated in Fig. 1. Assuming that the upper rock is disturbed by a spatially varying disturbance factor, the depth of the slip surfaces was determined, and the normalized thickness (T/T_0) is presented in Fig. 7(a) as a function of *GSI*. The infinite slope is assumed to be maximally disturbed at the slope face ($D_{max} = 1$), and the disturbance factor decreases linearly with depth ($k = 1$), ultimately reducing to zero at depth T_0. The result of $T/T_0 = 1$ indicates that the moving block includes the entire disturbed upper rock and slides on the lower undisturbed bedrock. When $GSI \geq 50$, this type of failure occurs irrespective of other parameters such as the slope inclination angle and m_i. Because the slip surface is on the interface (undisturbed rock) in such a case, the stability factor of rock with varying disturbances is identical to that of undisturbed rock, which is consistent with Fig. 6(a). For rocks with $GSI < 50$ and linearly decaying

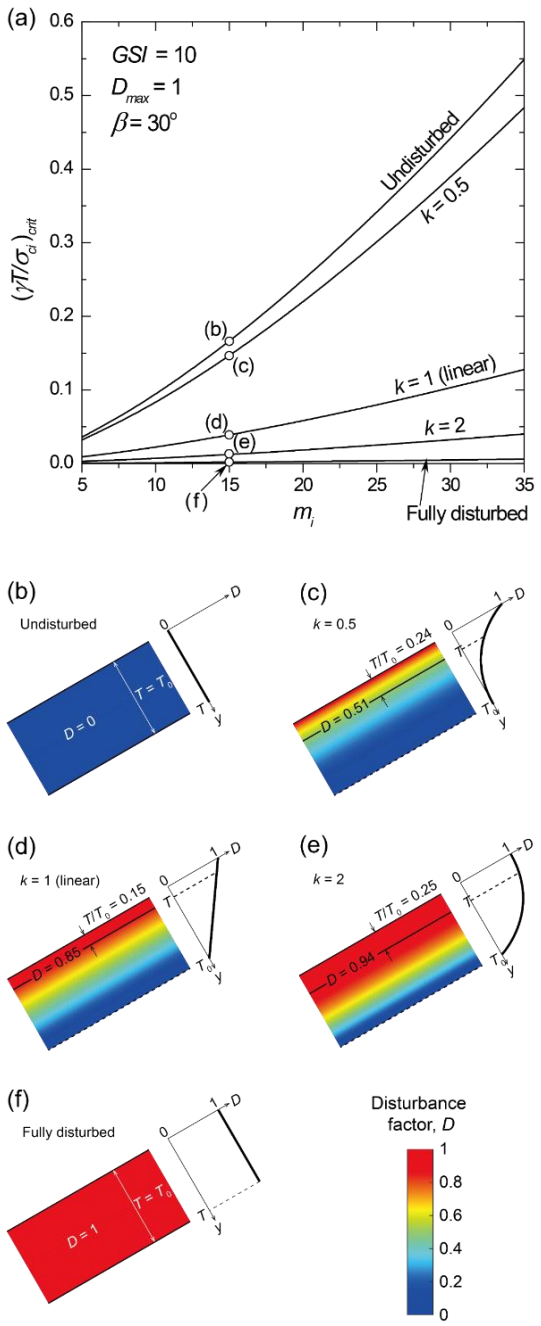

Fig. 8 Influence of spatial distribution of the disturbance factor on stability factor: (a) stability factor, and (b)-(f) failure mechanisms with different disturbance patterns

disturbances, the failure depth decreases with decreasing *GSI*. This is because the adverse effect of rock disturbance increases with a decrease in the *GSI*; thus, a slope can fail even at a shallow depth with a small rock weight (small driving force). For gentle slopes with $\beta = 30°$ (marked by the blue color in Fig. 7(a)), the corresponding failure mechanisms with $GSI = 10$, 30, 40, and 50 are illustrated in Figs. 7(b)-7(e), respectively. The associated disturbance factors on the slip surface were 0.85, 0.68, 0.49, and 0 ($T/T_0 = 0.15$, 0.32, 0.51, and 1, respectively). Disturbed rock slopes with different *GSI* values exhibit distinctly different failure patterns. A rock with a smaller *GSI*

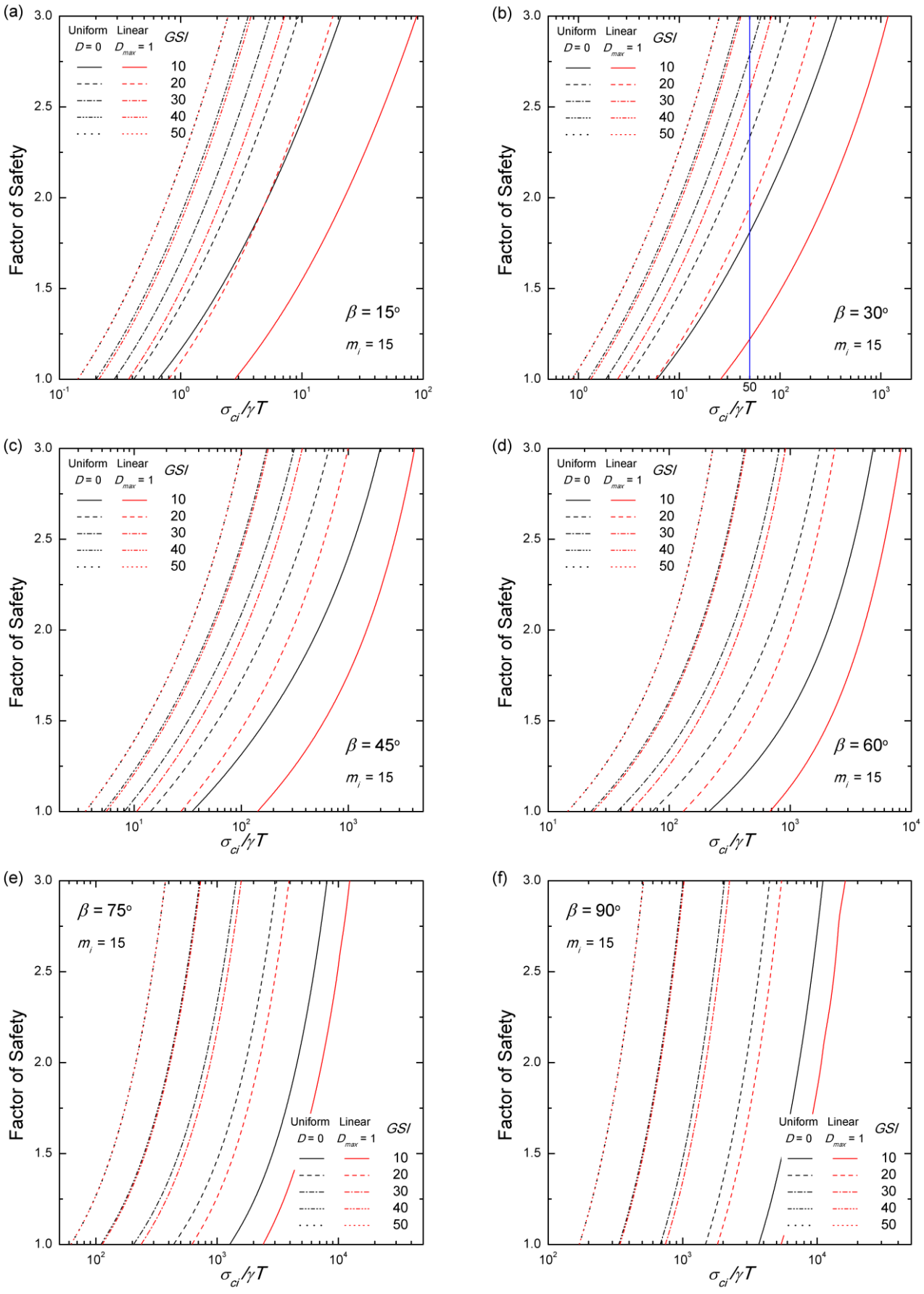

Fig. 1 Factor of safety: (a) $\beta = 15°$, (b) $\beta = 30°$, (c) $\beta = 45°$, (d) $\beta = 60°$, (e) $\beta = 75°$ and (f) $\beta = 90°$

Table 3 Factor of safety F for infinite rock slopes with $\beta = 30°$, $m_i = 15$, $\sigma_{ci}/\gamma T = 50$

Case*	*GSI*				
	10	20	30	40	50
A	1.81	2.33	2.79	3.23	3.74
B	1.22	1.95	2.59	3.19	3.74
C	0.45	0.82	1.21	1.64	2.14

*Case A: uniform $D = 0$ (undisturbed); Case B: $D_{max} = 1$ and $k = 1$ (linear); Case C: uniform $D = 1$ (fully disturbed)

corresponds to an infinite slope failure at a shallower depth where the rock is highly disturbed.

While a common assumption of the spatial distribution of the disturbance factor is a linear decaying function away from the source of disturbance, a different distribution of D was examined to investigate its influence on slope stability, as presented in Fig. 8. Fig. 8(a) shows the stability factors with different spatial variations of the disturbance factor calculated using Eq. (9) and the corresponding failure mechanisms are shown in Figs. 8(b)-8(f). The depth of the slip surface appears to be dependent on the spatial disturbance distribution; however, the interpretation is not straightforward. Among the cases considered, the linear decay function presents the smallest sliding rock mass (shallowest failure depth), as shown in Fig. 8(d). The failure depths of the nonlinear distributions of D characterized by $k = 0.5$ and 2 are deeper (Figs. 8(e)-8(e)) than that of the linear decrease. When uniform disturbance factors $D = 0$ or $D = 1$ are assumed, the thickness of the disturbed zone T_0 is not defined, and the critical depth T is directly obtained from the corresponding stability factor, $(\gamma T/\sigma_{ci})_{crit}$.

The factors of safety for infinite rock slopes in a disturbed rock mass can be determined by minimizing F in Eq. (18), and the results with $\beta = 15°$–$90°$ at intervals of 15° are presented in Figs. 9(a)-9(f). The factor of safety for an existing slope characterized by $\sigma_{ci}/\gamma T$ can be determined by reading the charts. The reciprocal of the dimensionless number $\sigma_{ci}/\gamma T$ at $F = 1$ (x-axis) is equivalent to the stability factor, indicating a state of limit equilibrium. For $\sigma_{ci}/\gamma T = 50$ and $\beta = 30°$ (Fig. 9(b)), the numerical values of the factors of safety are listed in Table 3. It also includes the results for the fully disturbed slopes ($D = 1$, Case C), which are not presented in Fig. 9(b). Unsurprisingly, the analysis with a uniformly disturbed rock slope yielded a substantial decrease in the factor of safety. For example, when $GSI = 10$, the factor of safety based on the realistic distribution of the disturbance factor (linear decrease) was 1.22. By assuming a fully disturbed rock mass with a single disturbance factor value ($D = 1$), it decreased to 0.45. The relative difference between Cases B and C decreased from 63% ($GSI = 10$) to 43% ($GSI = 50$) with increasing rock quality characterized by the *GSI*. This reduces to zero for intact rock with $GSI = 100$, where the disturbance factor does not affect the rock strength envelope.

A direct application of the proposed method to a specific engineering problem would be hindered without reliable field data used for calibrating the disturbance function in Eq. (9). However, it can be still fruitfully applicable to a safety assessment of the problem giving an immediate picture of the disturbance impact on the slope stability, along with charts and tables provided in this study. The focus of this study is on the analytical procedure for taking the spatially varying disturbance into the stability analysis for infinite slopes, and less on practical applications.

6. Conclusions

The rock mass is inevitably disturbed during excavation. In slope stability analyses, rock disturbance is considered using a uniform disturbance or parallel layer model, where a decreasing disturbance is assigned to a series of discrete layers. This study adopted a continuously decreasing disturbance factor with depth away from the source of disturbance and was devoted to the safety evaluation of infinite rock slopes. The following conclusions were drawn from this study.

1. The failure of infinite rock slopes is widespread; for example, weak rock is underlain by strong rock. When the upper rock layer is disturbed by blasting or stress relaxation, a potential slip surface is not necessarily at the interface between the disturbed rock and undisturbed bedrock but is located within the upper disturbed layer associated with the most susceptible condition.
2. In rocks with strength governed by the Hoek–Brown failure criterion, a low-quality rock characterized by a low *GSI* is more susceptible to the disturbance factor. When a very weak rock ($GSI = 10$) is maximally disturbed, both the tensile and compressive strengths of the rocks can be reduced by up to 83% from those of undisturbed strengths, whereas the strength of intact rock ($GSI = 100$) is not affected by the disturbance factor.
3. The computational results showed that assigning one value of D to the entire rock mass significantly underestimates the rock strength and, consequently, the safety of the rock slope. It can reduce the critical height by up to 95% compared to that of the linearly decreasing disturbance factor with depth, which is a realistic assumption. Analysis with uniform disturbance gives rise to excessive design at the expense of simple computation.
4. For infinite rock slopes with varying disturbance factors, a slip surface can form within the disturbed upper rock mass. This is a likely outcome of the decrease in the disturbance factor with depth, providing greater strength against slope failure.
5. It is interesting to note that when $GSI \geq 50$, the rock slope with a decreasing disturbance factor is equally stable to the undisturbed slope. This is because in medium to strong rock, the slip surface is in undisturbed rock at deep depths, and thus the disturbance near the slope face has no influence on slope safety. Consequently, the computation result is independent of the magnitude of the maximum disturbance factor at the slope face.
6. The most widely accepted safety measure that is the

factors of safety were calculated for infinite rock slopes by employing the parametric form of the Hoek–Brown failure criterion. The factor of safety is also significantly affected by rock disturbance and its spatial variation.

7. The slope stability analysis of disturbed rock slopes may not be difficult; however, quantitative characterization of the degree of disturbance, its extent, and decay rate is difficult. It is recommended that these parameters be adjusted based on field data and further verifications.

Acknowledgments

This work was supported by the 2021 Research Fund of the University of Seoul.

References

Balmer, G. (1952), "A general analysis solution for Mohr's envelope", *Proc. ASTM*, **52**, 1260-1271.

Cheng, Y., Song, Z., Song, W., Li, S., Yang, T., Zhang, Z., Wang, T. and Wang, K. (2021), "Strain performance and fracture response characteristics of hard rock under cyclic disturbance loading", *Geomech. Eng.*, **26**(6), 551-563. https://doi.org/10.12989/gae.2021.26.6.551.

Chern, J., Yu, C. and Shiao, F. (1998), "Tunnelling in squeezing ground and support estimation", *Proceedings of the Regional Symposium on Sedimentary Rock Engineering*, Taipei.

Chinaei, F., Ahangari, K. and Shirinabadi, R. (2021), "Hoek-Brown failure criterion for damage analysis of tunnels subjected to blast load", *Geomech. Eng.*, **26**(1), 41-47. https://doi.org/10.12989/gae.2021.26.1.041.

Das, B.M. (2021), *Principles of Geotechnical Engineering*. Cengage learning, Stamford, CT, USA.

Dimitraki, L.S., Christaras, B.G. and Arampelos, N.D. (2021), "Investigation of blasting impact on limestone of varying quality using FEA", *Geomech. Eng.*, **25**(2), 111-121. https://doi.org/10.12989/gae.2021.25.2.111.

Dong-ping, D., Liang, L., Jian-feng, W. and Lian-heng, Z. (2016), "Limit equilibrium method for rock slope stability analysis by using the Generalized Hoek–Brown criterion", *Int. J. Rock Mech. Min. Sci.*, **89**, 176-184. https://doi.org/10.1016/j.ijrmms.2016.09.007.

Duncan, J.M., Wright, S.G. and Brandon, T.L. (2014), *Soil strength and slope stability*. John Wiley & Sons, Hoboken, NJ, USA.

Hoek, E. (1994), "Strength of rock and rock masses", *ISRM News J.*, **2**, 4-16.

Hoek, E. (2012), "Blast damage factor D", *Technical note for RocNews-February 2*.

Hoek, E. and Brown, E. (2019), "The Hoek–Brown failure criterion and GSI–2018 edition", *J. Rock Mech. Geotech. Eng.*, **11**(3), 445-463. https://doi.org/10.1016/j.jrmge.2018.08.001.

Hoek, E. and Brown, E.T. (1980), "Empirical strength criterion for rock masses", *J. Geotech. Geoenviron. Eng.*, **106**(9), 1013-1035. https://doi.org/10.1061/AJGEB6.0001029.

Hoek, E. and Brown, E.T. (1988), "The Hoek-Brown failure criterion–a 1988 update", *Proceedings of the 15th Can. Rock Mech. Symp*., Toronto, Canada, October.

Hoek, E. and Brown, E.T. (1997), "Practical estimates of rock mass strength", *Int. J. Rock Mech. Min. Sci.*, **34**(8), 1165-1186. https://doi.org/10.1016/S1365-1609(97)80069-X.

Hoek, E., Carranza-Torres, C. and Corkum, B. (2002), "Hoek-Brown failure criterion-2002 edition", *Proceedings of NARMS-Tac*, **1**(1), 267-273.

Hoek, E. and Karzulovic, A. (2000), "Rock mass properties for surface mines", *Slope Stability in Surface Mining,* Denver, CO, USA, Febrary.

Hoek, E. and Marinos, P. (2007), "A brief history of the development of the Hoek-Brown failure criterion", *Soils Rocks*, **2**(2), 2-13.

Hsu, S.C. and Nelson, P.P. (2006), "Material spatial variability and slope stability for weak rock masses", *J. Geotech. Geoenviron. Eng.*, **132**(2), 183-193. https://doi.org/10.1061/(ASCE)1090-0241(2006)132:2(183).

Kumar, P. (1998), "Shear failure envelope of Hoek-Brown criterion for rockmass", *Tunn. Undergr. Sp. Technol.*, **13**(4), 453-458. https://doi.org/10.1016/S0886-7798(98)00088-1.

Kwon, S., Lee, C., Cho, S., Jeon, S. and Cho, W. (2009), "An investigation of the excavation damaged zone at the KAERI underground research tunnel", *Tunn. Undergr. Sp. Technol.*, **24**(1), 1-13. https://doi.org/10.1016/j.tust.2008.01.004.

Lambe, T.W. and Whitman, R.V. (1969), *Soil mechanics*, John Wiley, New York, NY, USA.

Li, A., Merifield, R. and Lyamin, A. (2011), "Effect of rock mass disturbance on the stability of rock slopes using the Hoek–Brown failure criterion", *Comput. Geotech.*, **38**(4), 546-558. https://doi.org/10.1016/j.compgeo.2011.03.003.

Lupogo, K. (2017), "Characterization of blast damage in rock slopes: an integrated field-numerical modeling approach", Ph.D. Dissertation, Simon Fraser University, British Columbia.

Michalowski, R.L. (2018), "Failure potential of infinite slopes in bonded soils with tensile strength cut-off", *Can. Geotech. J.*, **55**(4), 477-485. https://doi.org/10.1139/cgj-2017-0041.

Michalowski, R.L. and Park, D. (2020), "Stability assessment of slopes in rock governed by the Hoek-Brown strength criterion", *Int. J. Rock Mech. Min. Sci.*, **127**, 104217. https://doi.org/10.1016/j.ijrmms.2020.104217.

Park, D. and Michalowski, R.L. (2019), "Roof stability in deep rock tunnels", *Int. J. Rock Mech. Min. Sci.*, **124**, 104139. https://doi.org/10.1016/j.ijrmms.2019.104139.

Park, D. and Michalowski, R.L. (2020), "Three-dimensional roof collapse analysis in circular tunnels in rock", *Int. J. Rock Mech. Min. Sci.*, **128**, 104275. https://doi.org/10.1016/j.ijrmms.2020.104275.

Park, D. and Michalowski, R.L. (2021), "Three-dimensional stability assessment of slopes in intact rock governed by the Hoek-Brown failure criterion", *Int. J. Rock Mech. Min. Sci.*, **137**, 104522. https://doi.org/10.1016/j.ijrmms.2020.104522.

Park, D. and Michalowski, R.L. (2022), "Roof stability in flat-ceiling deep rock cavities and tunnels", *Eng. Geol.*, **303**, 106651. https://doi.org/10.1016/j.enggeo.2022.106651.

Qian, Z., Li, A.J., Lyamin, A. and Wang, C. (2017), "Parametric studies of disturbed rock slope stability based on finite element limit analysis methods", *Comput. Geotech.*, **81**, 155-166. https://doi.org/10.1016/j.compgeo.2016.08.012.

Rafiei Renani, H., Martin, C.D., Varona, P. and Lorig, L. (2019), "Stability analysis of slopes with spatially variable strength properties", *Rock Mech. Rock Eng.*, **52**(10), 3791-3808. https://doi.org/10.1007/s00603-019-01828-2.

Rankine, W.J.M. (1857), "II. On the stability of loose earth", *Philos. T. Roy. Soc. London*, **147**, 9-27.

Rose, N., Scholz, M., Burden, J., King, M., Maggs, C. and Havaej, M. (2018), "Quantifying transitional rock mass disturbance in open pit slopes related to mining excavation", *Proceedings of the 14th International Congress on Energy and Mineral Resources*, Seville, Spain, April.

Sakurai, S. (1984), "Displacement measurements associated with the design of underground openings", *Field measurements in*

geomechanics. Zurich, Switzerland, September.

Serrano, A., Olalla, C. and Manzanas, J. (2005), "Stability of highly fractured infinite rock slopes with nonlinear failure criteria and nonassociated flow laws", *Can. Geotech. J.*, **42**(2), 393-411. https://doi.org/10.1139/t04-087.

Song, K.I., Cho, G.C. and Lee, S.W. (2011), "Effects of spatially variable weathered rock properties on tunnel behavior", *Probabilist. Eng. Mech*., **26**(3), 413-426. https://doi.org/10.1016/j.probengmech.2010.11.010.

Sonmez, H. and Ulusay, R. (1999), "Modifications to the geological strength index (GSI) and their applicability to stability of slopes", *Int. J. Rock Mech. Min. Sci.*, **36**(6), 743-760. https://doi.org/10.1016/S0148-9062(99)00043-1.

Sun, C., Chai, J., Xu, Z., Qin, Y. and Chen, X. (2016), "Stability charts for rock mass slopes based on the Hoek-Brown strength reduction technique", *Eng. Geol.*, **214**, 94-106. https://doi.org/10.1016/j.enggeo.2016.09.017.

Taylor, D.W. (1937), "Stability of earth slopes", *J. Boston Soc. Civil Engineers*, **24**(3), 197-247.

Yang, J., Dai, J., Yao, C., Jiang, S., Zhou, C. and Jiang, Q. (2020), "Estimation of rock mass properties in excavation damage zones of rock slopes based on the Hoek-Brown criterion and acoustic testing", *Int. J. Rock Mech. Min. Sci.*, **126**, 104192. https://doi.org/10.1016/j.ijrmms.2019.104192.

Zaid, M., Sadique, M.R., Alam, M.M. and Samanta, M. (2020), "Effect of shear zone on dynamic behaviour of rock tunnel constructed in highly weathered granite", *Geomech. Eng.*, **23**(3), 245-259. https://doi.org/10.12989/gae.2020.23.3.245.

Zheng, H., Li, T., Shen, J., Xu, C., Sun, H. and Lü, Q. (2018), "The effects of blast damage zone thickness on rock slope stability", *Eng. Geol.*, **246**, 19-27. https://doi.org/10.1016/j.enggeo.2018.09.021.